Applied Catalysis B: Environmental 180 (2016) 580–585

Contents lists available at ScienceDirect

Applied Catalysis B: Environmental

journal homepage: www.elsevier.com/locate/apcatb

Highly selective hydrogenation of furfural over supported Pt nanoparticles under mild conditions

Martin J. Taylor[a], Lee J. Durndell[b], Mark A. Isaacs[b], Christopher M.A. Parlett[b], Karen Wilson[b], Adam F. Lee[b], Georgios Kyriakou[a,*]

[a] Department of Chemistry, The University of Hull, Cottingham Rd., Hull HU6 7RX, United Kingdom
[b] European Bioenergy Research Institute, Aston University, Aston Triangle, Birmingham B4 7ET, United Kingdom

ARTICLE INFO

Article history:
Received 21 April 2015
Received in revised form 29 June 2015
Accepted 7 July 2015
Available online 15 July 2015

Keywords:
Platinum
Hydrogenation
Furfural
Ambient conditions
Supported catalysts

ABSTRACT

The selective liquid phase hydrogenation of furfural to furfuryl alcohol over Pt nanoparticles supported on SiO_2, ZnO, γ-Al_2O_3, CeO_2 is reported under extremely mild conditions. Ambient hydrogen pressure, and temperatures as low as 50 °C are shown sufficient to drive furfural hydrogenation with high conversion and >99% selectivity to furfuryl alcohol. Strong support and solvent dependencies are observed, with methanol and *n*-butanol proving excellent solvents for promoting high furfuryl alcohol yields over uniformly dispersed 4 nm Pt nanoparticles over MgO, CeO_2 and γ-Al_2O_3. In contrast, non-polar solvents conferred poor furfural conversion, while ethanol favored acetal by-product formation. Furfural selective hydrogenation can be tuned through controlling the oxide support, reaction solvent and temperature.
© 2015 Elsevier B.V. All rights reserved.

1. Introduction

Sustainable low carbon biofuels derived from lignocellulosic or oleochemical biomass sources are urgently sought [1–3] to address climate change and energy security issues arising from the availability of usable versus unburnable [4] non-renewable fossil fuels. The quest for sustainable biofuels also impacts upon the broader chemicals industry, since the overwhelming proportion of carbon feedstocks they employ today obtain from petroleum and natural gas. In this respect, the development of the bio-refinery concept for the co-production of sustainable fuels and chemicals has the power to transform global energy and materials markets, but necessitates the development of new catalytic processes capable of selectively transforming biomass derived oxygenated organics into either alternative 'drop in' chemical intermediates and fuels, or entirely products with novel properties.

Among these oxygenates, furfural and its derivatives are promising starting materials and building blocks from which to synthesize high volume products such as polyols, which find direct application as monomer precursors for the polyester industry, or the production of polyamides or polyurethenes via respective oxidation or amination [5,6]. Fufural hydrogenation to furfuryl alcohol, an intermediate to the manufacture of lysine, ascorbic acid and numerous lubricants [7] represents a key synthetic transformation for furfural exploitation (Fig. 1), and one wherein there is significant academic and commercial interest in new energy efficient routes. Approximately 62% of furfural currently produced is converted into furfuryl alcohol [6]. The present industrial process for furfural hydrogenation to furfuryl alcohol employs a copper chromate catalyst [8], operating between 130 and 200 °C, at pressures up to 30 bar. While copper chromate exhibits good activity and selectivity towards furfuryl alcohol, the use of toxic Cr_2O_3, whose disposal is prohibited in landfill sites, is highly undesirable, hence the driver for energy efficient alternative catalytic processes operating at mild temperature and pressure and utilizes less toxic components [9–11].

A variety of precious metal catalysts have been investigated for the gas phase and liquid phase hydrogenation of furfural, including Ni, Ru, Pd, Co, Cu and Pt [6,7,12–16]. Platinum in particular has drawn recent attention for the vapor phase hydrogenation of furfural by Somorjai and co-workers [17–19] over SiO_2, Al_2O_3, TiO_2, Nb_2O_5 and Ta_2O_5 mesoporous oxide supports, highlighting the importance of particle size effects; Pt nanoparticles <3 nm favored furfural decarbonylation to furan, whereas those between 3 and

* Corresponding author.
E-mail address: G.Kyriakou@hull.ac.uk (G. Kyriakou).

http://dx.doi.org/10.1016/j.apcatb.2015.07.006
0926-3373/© 2015 Elsevier B.V. All rights reserved.

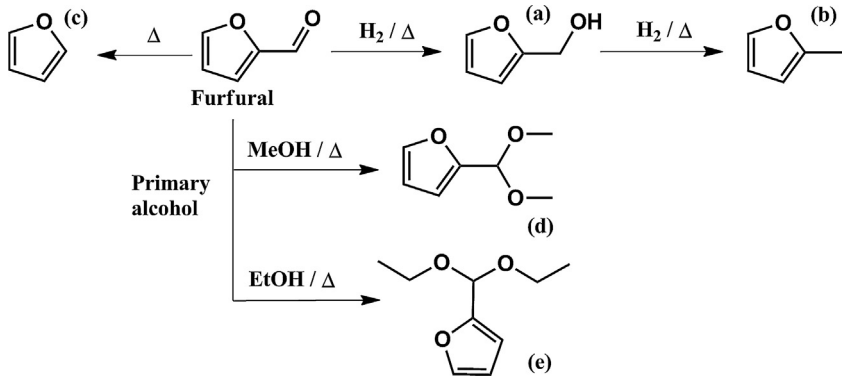

Fig. 1. Furfural reaction scheme containing both hydrogenation and coupling reactions occurring with alcohol based solvents. (a) furfuryl alcohol, (b) methyl furan, (c) furan, (d) 2-furaldehyde dimethyl acetal and (e) 2-furaldehyde diethyl acetal.

7 nm promoted hydrogenation to furfuryl alcohol [13,17]. Sum frequency spectroscopy studies also indicate that metal-support interactions are important for Pt nanoparticles on TiO_2, facilitating hydrogen spillover and the concomitant formation of a furfuryl-oxy intermediate over titania [18,19]. The influence of surface polarity upon the Pt catalyzed selective hydrogenation of allylic aldehydes was also recently reported over silica supports [20].

Here we investigate the selective hydrogenation of furfural to furfuryl alcohol under extremely mild reaction conditions over Pt nanoparticles supported on SiO_2, ZnO, γ-Al_2O_3, CeO_2 and MgO. Strong support and solvent dependencies were observed, with methanol and *n*-butanol proving excellent solvents for promoting high furfuryl alcohol yields over uniformly dispersed Pt nanoparticles when using MgO, CeO_2 and γ-Al_2O_3 as supports at 50 °C and atmospheric hydrogen pressure. In contrast, non-polar solvents conferred poor furfural conversion, while ethanol favored acetal by-product formation, as commonly reported in the literature [12,21–25].

2. Experimental

2.1. Synthesis

Colloidal Pt nanoparticles were prepared adapting the method of Jones et al. [26], employing a $H_2PtCl_6{\cdot}H_2O$ precursor since residual chlorine has been found to have a promotional effect in the selective hydrogenation of α,β-unsaturated aldehydes [27]. To a stirred 10 ml aliquot of ethylene glycol (Fisher >99%) at 120 °C, 50 μl of 0.1 M aqueous sodium hydroxide solution was added to promote nucleation. To the hot glycol, a solution of $H_2PtCl_6 \times H_2O$ (10.6 mM, Alfa Aesar, 99.9%) and polyvinylpyrrolidone (PVP) (91 mM, Alfa Aesar) in a 9:1 per volume ethylene glycol:water mixture was added slowly over the course of an hour resulting in a color change from light brown to black. The reaction mixture was stirred for an additional 20 min and then cooled to room temperature. Nanoparticles were isolated by the addition of acetone (three times the reaction volume) followed by subsequent centrifugation at 3500 rpm. This process was repeated three times and the nanoparticles then dispersed in ethanol before supporting on oxide supports: SiO_2 (Alfa Aesar amorphous fumed, 175–225 $m^2\,g^{-1}$); γ-Al_2O_3 (Alfa Aesar 99.5%, 32–40 $m^2\,g^{-1}$), CeO_2 (Alfa Aesar 99.5%, 3 $m^2\,g^{-1}$), MgO (Alfa Aesar, 99+%, >7 $m^2\,g^{-1}$) and ZnO (Alfa Aesar, 99.9%, 10 $m^2\,g^{-1}$). Supports were not pretreated prior to platinum deposition. The resulting slurries were slowly dried in vacuo, and the dried powders then transferred to a tube furnace and heated at 3 °C min^{-1} under air (60 $cm^3\,min^{-1}$) to 300 °C for 4 h to remove the PVP stabiliser and immobilise the Pt nanoparticles. The resulting materials were reduced at 200 °C in flowing 10% H_2/N_2 for 1 h, cooled and stored in air.

2.2. Characterization of catalysts

All samples were analysed via a JEOL 2010 Transmission Electron Microscopy (TEM) operated at 200 kV, with STEM were recorded using a C_s aberration-corrected JEOL 2100F microscope at 200 kV. Images were collected using a Gatan Ultrascan 4000 digital camera operated by Digital Micrograph software. Samples were dispersed in ethanol and deposited on 300-mesh carbon-supported copper grids and dried under ambient conditions Metal contents were determined by inductively coupled plasma optical emission spectroscopy (ICP-OES, PerkinElmer Optical Emission Spectrometer Optima 5300 DV) after microwave digestion of the samples in 2 ml HNO_3 (Romil SPA grade 70%), 2 ml HCl (Romil SPA grade 60%), and depending on the oxide, 2 ml HF (Romil SPA grade 40%) at 200 °C (CEM–MARS microwave reactor) followed by aqueous dilution. Bulk compositions are ±10%. BET surface areas were determined via N_2 physisorption using a Micromeritics TriStar porosimeter. X-ray photoelectron spectra were acquired on a Kratos AXIS HSi spectrometer equipped with a charge neutralizer and monochromated Al Kα excitation source (1486.7 eV), with energies referenced to adventitious carbon at 284.6 eV. Spectral fitting was performed using CasaXPS version 2.3.15. Powder X-ray diffraction was performed on a Bruker D8 Advance diffractometer using monochromated Cu $K\alpha_1$ radiation (λ = 0.1542 nm). Subsequent peak assignment was based on the ICDD's PDF-2 2012 database.

2.3. Catalytic testing

Catalytic hydrogenation was performed using a 12-port Radleys Plus Reaction Station. Reaction tubes were first evacuated and purged with hydrogen (Energas 99.99%) three times to ensure that the system was air-free; hydrogen was supplied via balloons pressurised to 1.02 atm, as measured by a Measurement Specialties™ XP5 pressure sensor. In a typical run, 10 ml of solvent, 16.5 μl (approximately 0.02 mmols) of furfural and 20 mg of catalyst were mixed at 600 rpm. The reaction mixture was sampled at measured time intervals with quantification via an external dodecane standard and analysis on a Bruker Scion 456-GC equipped with a flame ionisation detector and a Zebron ZB-5 (5%-phenyl-95%-dimethylpolysiloxane) capillary column. GC–MS was performed using an Agilent 6890 GC equipped with an Agilent 5973N Quadrupole mass spectrometer and an RXI-5MS (5%-phenyl-95%-dimethylpolysiloxane) capillary column. Product selectivity was determined according to Eq. S1, with carbon mass

Table 1
Bulk elemental analysis and surface area measurements of Pt catalysts.

Catalyst	Pt loading[a]/wt%	Surface area[b]/m^2 g^{-1}
Pt/SiO_2	2.0	181
$Pt/\gamma\text{-}Al_2O_3$	1.9	34
Pt/MgO	2.3	12
Pt/CeO_2	1.4	5
Pt/ZnO	1.9	7

[a] Determined by ICP-OES; [b]BET surface area from N_2 porosimetry.

Table 2
Surface Pt metal concentration and Pt loading from XPS.

Sample	Pt^0/%	Surface Pt loading/wt%
2.0% Pt/SiO_2	61.3	0.9
1.9% $Pt/\gamma\text{-}Al_2O_3$	72.6	14.3
2.3% Pt/MgO	71.7	10.3
1.9% Pt/ZnO	96.2	32.1
1.4% Pt/CeO_2	85.0	48.7

balances ~98%, and errors in reported conversion and selectivity of ±2%.

3. Results and discussion

3.1. BET, ICP-OES, TEM, PXRD and XPS

Table 1 shows elemental analysis and surface area measurements for the five supported Pt catalysts after calcination and reduction, from which it is apparent that the final Pt content was close to the nominal 2 wt% over SiO_2, $\gamma\text{-}Al_2O_3$ and ZnO supports, and only deviated slightly from this for the CeO_2 and MgO supports. Although the surface areas of the parent supports spanned a wide range, there was minimal change for any of the five catalysts following particle deposition, calcination and reduction treatments relative to the parent value.

Fig. 2 shows TEM images and corresponding particle size distributions for the unsupported, PVP-stabilised Pt nanoparticles, and oxide supported analogues following thermal processing. The unsupported Pt-PVP nanoparticles exhibited mean particle diameters of 3.9 ± 0.8 nm. Similar dimensions were observed for the thermally processed, supported Pt nanoparticles on $\gamma\text{-}Al_2O_3$ (4.0 ± 0.5 nm), CeO_2 (4.2 ± 0.6 nm) and MgO (3.9 ± 0.5 nm). The size distribution diagrams shown in Fig. 2c–e show that the overall distribution is tight and the particles are relatively homogeneously distributed. The Pt particle size distribution on SiO_2 was substantially broader with a larger mean diameter of 6.0 ± 1.0 nm, which likely reflects a weaker interaction with the silica support and resultant mild sintering [28,29]. For the Pt/ZnO catalyst, the particle size distribution was also centered around 3.8 nm (±0.9 nm), albeit with a significant number of smaller 1–3 nm particles also present. This is depicted in the histograms shown in Fig. 2 which shows a relatively broad distribution for these two samples leading to a larger standard deviation on the particle size. With the exception of SiO_2, TEM demonstrated that mild calcination (300 °C) and reduction (200 °C) steps induced minimal agglomeration or growth of deposited Pt nanoparticles, essential to isolate the influence of the different supports. Ramos-Fernández et al. demonstrated that in the case of Pt/ZnO, higher reduction temperatures of 350 °C promoted particle agglomeration and deactivation in the hydrogenation of cinnamaldehyde [30]. As discussed later, the small apparent difference in nanoparticle size distribution over SiO_2, and the presence of some smaller particles over ZnO, exerts a significant influence upon the resulting catalytic performance of these two supports relative to the other oxide supports.

Powder X-ray diffraction was also performed on all Pt catalysts (Fig. S1). The samples show no evidence of Pt particles due to both the low metal loading and small particle size. This does however show that the catalyst furnace treatment in both air and dilute hydrogen has no effect on the morphology of the oxide supports which present the expected X-ray diffraction pattern. The diffractogram of $\gamma\text{-}Al_2O_3$ shows trace amounts of $\delta\text{-}Al_2O_3$ impurities and the SiO_2 support appears to be amorphous in nature.

Table 2 shows the XPS derived Pt surface loading and metal content. The Pt4f spectra are shown in Fig. S2. The observed surface Pt loading was inversely proportional to the support surface area, reflecting a greater proportion of nanoparticles dispersed over the external surface of (largely non-porous) MgO, CeO_2 and ZnO. Fig. S3(a and b) shows bright- and dark-field STEM images of Pt/SiO_2

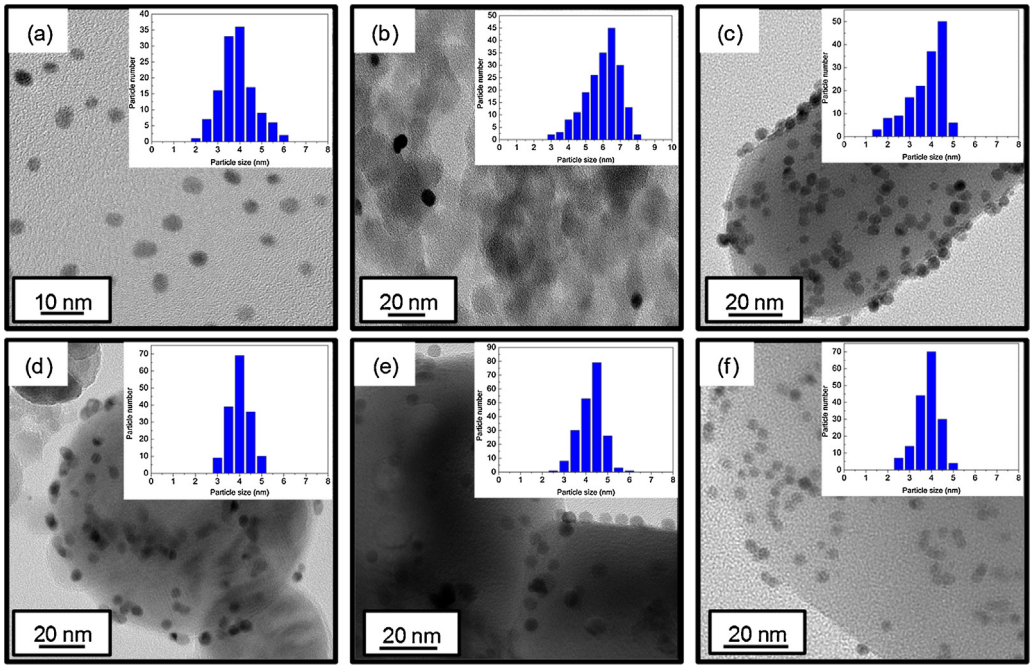

Fig. 2. TEM images and particle size distribution of; (a) unsupported Pt particles, (b) Pt/SiO_2, (c) Pt/ZnO, (d) $Pt/\gamma\text{-}Al_2O_3$, (e) Pt/CeO_2 and (f) Pt/MgO.

Table 3
Furfural hydrogenation over Pt catalysts after 7 h reaction in ethanol at 70 °C; 2-furaldehyde diethyl acetal expressed as Solvent Product (SP).

Catalyst	Furfural conversion/%	Furfuryl alcohol selectivity/%	Furan selectivity/%	SP selectivity/%
Pt/γ-Al_2O_3	58	72	3	25
Pt/MgO	45	93	6	1
Pt/CeO_2	97	27	3	70
Pt/SiO_2	24	75	8	17
Pt/ZnO	8	9	91	0

showing the low density of nanoparticles across the higher area support, in contrast to Pt/CeO_2 wherein the high surface Pt loading (48.7 wt%) from XPS is consistent with a higher surface density of Pt nanoparticles (Fig. S3(c and d)). In all cases the as-prepared catalysts contained a high proportion of metallic platinum following reductive pretreatment as expected. TPR proved uninformative due to the low concentration of surface platinum oxide present on our predominantly metallic nanoparticles and contributions arising from the reducible metal oxide supports.

3.2. Catalytic reaction testing

The performance of the preceding five catalysts was first investigated for the hydrogenation of furfural at 70 °C with ethanol as the solvent. In all cases, the desired selective hydrogenation product furfuryl alcohol was observed, alongside furan and 2-furaldehyde diethyl acetal (Table 3). The latter is a side-product of reaction between furfural and the alcohol solvent, whose formation hinders the maximum selectivity achievable. Furfural conversion decreased in the order Pt/CeO_2 > Pt/γ-Al_2O_3 > Pt/MgO > Pt/SiO_2 > Pt/ZnO, while the selectivity to furfuryl alcohol varied between 9 and 70%, decreasing in the order Pt/MgO > Pt/SiO_2 > Pt/γ-Al_2O_3 > Pt/CeO_2 > Pt/ZnO. The relatively low activity of the Pt/ZnO catalyst was accompanied by the formation of furan arising from furfural decarbonylation, as observed by Somorjai and co-workers who reported that PVP-stabilised Pt nanoparticles dispersed on mesoporous oxides including Al_2O_3, TiO_2, Nb_2O_5 and Ta_2O_5 favored furan during vapor phase transformations of furfural [17,19]. The choice of oxide support, and/or precise nanoparticle size distribution, strongly influences the side reaction between furfural and the solvents.

The acetalization of aldehydes, including furfural, in alcoholic solvents is commonly reported in the literature (Schematic S1), but is often unquantified [12,22–25,31]. Notably the addition of water forces the back reaction to furfural. The addition of base has also been found to hinder the reaction as the acetalization process is acid catalyzed [24,25]. Merlo and co-workers reported an ether side product, 2-isopropoxymethylfuran, during furfural hydrogenation in 2-propanol at 10 bar and 100 °C, formed with 3.6% selectivity over a PtSn catalyst and 22% over NiSn catalyst [22,23,32]. Similar observations were made by Vaidya et al. in the same solvent for furfural hydrogenation under 20 bar hydrogen and 150 °C [12]. Furfural acetalization with methanol was also reported using a Ni based catalyst during hydrogenation [33], while 2-furaldehyde diethyl acetal has been previously observed using ethanol as the solvent in furfural hydrogenation [22].

In the absence of any solid catalyst, neither hydrogenation nor decarbonylation reactions were observed in the present work, although significant furfural reacted with ethanol to form 2-furaldehyde diethyl acetal (61% yield after 7 h). The parent supports were also inactive towards furfural hydrogenation (Table S1), favoring either decarbonylation to furan or acetalization with ethanol. Interestingly, the acetalization reaction on the untreated supports was found to be inhibited in most cases due to inherent water present. The extent of the acetalization observed with the bare supports was strongly dependant on the degree of hydration of the bare support. Furfural reaction over all the Pt/oxide catalysts (except Pt/CeO_2 which attained complete conversion) reached a plateau in their conversions and selectivities after 7 h reaction, indicative of either catalyst deactivation or mass-transport limitation effects (Fig. S4). In the case of Pt/SiO_2 and Pt/CeO_2 there was some evidence for competition between furfural hydrogenation to furfuryl alcohol versus acetalization, with their respective selectivities exhibiting a weak anti-correlation. It is interesting to note that the acetalization side reaction, generally considered to be acid catalyzed, was suppressed over the most basic Pt/MgO and Pt/ZnO catalysts [34,35].

Table 4
Influence of solvent on furfural hydrogenation over Pt/γ-Al_2O_3 after 7 h reaction at 70 °C; 2-furaldehyde diethyl acetal (ethanol) and 2-furaldehyde dimethyl acetal (methanol) expressed as Solvent Product (SP).

Solvent	Furfural conversion/%	Furfuryl alcohol selectivity/%	Furan selectivity/%	SP selectivity/%
Methanol	65	77	19	5
Ethanol	62	73	2	25
n-Butanol	45	52	48	0
Toluene	49	21	79	0
Hexane	2	71	29	0

Table 5
Furfural hydrogenation over Pt catalysts after 7 h reaction in methanol at 50 °C; 2-furaldehyde dimethyl acetal expressed as Solvent Product (SP).

Catalyst	Furfural conversion/%	Furfuryl alcohol selectivity/%	Furan selectivity/%	SP selectivity/%
Pt/γ-Al_2O_3	80	99	1	0
Pt/MgO	79	97	3	0
Pt/CeO_2	77	98	1	1
Pt/SiO_2	35	90	7	3
Pt/ZnO	7	60	40	0

As a result of the acetalization observed during reaction in ethanol, a range of alternative solvents were investigated to determine whether acetalization could be suppressed while maintaining high rates for the primary hydrogenation of furfural to furfuryl alcohol. Since Pt/γ-Al_2O_3 was only moderately active towards furfural acetalization in ethanol it was selected for screening against other alcohol and non-polar solvents. The results are summarized in Table 4. Non-polar toluene and hexane resulted in low furfural conversion, and comparatively high degrees of decarbonylation to furan, in accordance with previous higher pressure studies of Pt/SiO_2 and PtSn/SiO_2 catalysts [22], which may reflect their poor hydrogen solubilities. Amongst the alcohols, selectivity to furfuryl alcohol decreased significantly with increasing solvent chain length, with n-butanol producing high yields of furan. Selectivity towards the undesired acetal side product decreased from ethanol » methanol > *n*-butanol. In the case of methanol, small amounts of 2-furaldehyde dimethyl acetal were observed after 7 h, while acetal formation was not detectable using *n*-butanol as the solvent (Table 4), and hence these solvents are better suited for furfural hydrogenation. This trend in acetalization reactivity is similar to that reported in the absence of catalyst [35–37].

Having identified methanol as the most suitable solvent for furfural hydrogenation, the impact of reaction temperature on selectivity to furfuryl alcohol was subsequently explored over the different oxide supports in an effort to further suppress the solvent side reaction. Lowering the reaction temperature from 70 to 50 °C surprisingly *increased* activity, in addition to enhancing furfuryl alcohol selectivity (Table 5) to >90% for all the supports except ZnO. Indeed, under these exceptionally mild pressure and temperature conditions, Pt/CeO_2 and Pt/γ-Al_2O_3 delivered approximately 80% furfural conversion at 99% furfuryl alcohol selectivity. A com-

Table 6
Furfural hydrogenation over recycled Pt catalysts after 7 h reaction in methanol at 50 °C; 2-furaldehyde dimethyl acetal expressed as Solvent Product (SP).

Catalyst	Furfural conversion/%	Furfuryl alcohol selectivity/%	Furan selectivity/%	SP selectivity/%
$^{2}Pt/\gamma\text{-}Al_2O_3$	79	97	0	3
$^{3}Pt/\gamma\text{-}Al_2O_3$	78	97	0	3
$^{2}Pt/MgO$	76	96	4	0
$^{3}Pt/MgO$	75	96	4	0
$^{2}Pt/CeO_2$	73	96	1	3
$^{3}Pt/CeO_2$	71	95	0	5
$^{2}Pt/SiO_2$	30	89	5	6
$^{3}Pt/SiO_2$	29	81	9	10
$^{2}Pt/ZnO$	0.6	40	44	16
$^{3}Pt/ZnO$	0.1	31	51	18

Where: 2 – 2nd cycle of testing, 3 – 3rd cycle of testing.

parison of $Pt/\gamma\text{-}Al_2O_3$ at 50 °C and 70 °C reveals acetal formation as strongly temperature dependent.

The poorer activity of the Pt/ZnO catalyst arises from contributions of the ZnO support, which was found to favor decarbonylation, (Table S1) and possibly due to a the relatively larger number of small Pt particles which may lead to site-blocking of the Pt sites by strongly bound CO [17]. Similar CO poisoning was reported for SiO_2 supported Group VIII metals during the liquid phase hydrogenation of citral [38]. Pt/SiO_2 exhibited activity intermediate between ZnO and the other oxides, however, it retained high selectivity towards furfuryl alcohol, and hence the poorer activity over silica is attributed to the larger Pt nanoparticles present hence lower reactive surface area. Interestingly, Pt/MgO and Pt/SiO_2 catalysts, which possess a relatively high number of $\leq$3 nm particles, favour furan formation relative to $Pt/\gamma\text{-}Al_2O_3$and Pt/CeO_2. These results suggest that under our reaction conditions, selectivity in furfural hydrogenation is particle size dependent, with monodispersed Pt nanoparticles ~4 nm possessing optimal activity and selectivity.

At 50 °C, metal-support interactions, or direct catalysis by the support, appear relatively unimportant since identically sized nanoparticulate Pt behaves similarly on CeO_2, $\gamma\text{-}Al_2O_3$ and MgO, three widely different supports. However, the nature of the oxide support appears to be crucial in respect of regulating the dispersion of Pt nanoparticles, and hence regulating furfural decarbonylation versus selective hydrogenation.

The recyclability of the catalysts was also investigated. All catalysts were reclaimed after reaction via centrifugation, followed by a methanol wash and further centrifuging. The catalysts were then left to dry at room temperature. Once dry they were retested under identical conditions to those reported in Table 5. This process was repeated in two successive cycles. Table 6 shows that for the $Pt/\gamma\text{-}Al_2O_3$, Pt/CeO_2, Pt/MgO and Pt/SiO_2 there is a marginal drop in activity as compared to Table 5 while the selectivity to furfuryl alcohol remains at the same levels. As previously postulated, Pt/ZnO appears to self-poison due to decarbonylation of furfural on ZnO support leading to Pt poisoning.

4. Conclusions

The platinum catalyzed liquid phase hydrogenation of furfural was studied over five different oxide supports under mild reaction conditions. A simple and reproducible method was developed to support a narrow size distribution of stabiliser-free Pt nanoparticles over SiO_2, ZnO, $\gamma\text{-}Al_2O_3$, CeO_2 and MgO. Furfural hydrogenation was sensitive to Pt particle size, with those of approximately 4 nm highly active and selective for the hydrogenation reaction in methanol, even at 50 °C, whereas smaller Pt nanoparticles present in the MgO and SiO_2 catalysts promote some decarbonylation to furan. Indeed for Pt/ZnO, extensive decarbonylation over the ZnO support appears to dominate Pt catalysis. The reaction is also strongly sensitive to the solvent selection, with alcohols more active than non-polar solvents. However, certain alcohols such as ethanol favor the formation of undesired acetal side products through reaction with furfural at 70 °C, although such competing reactions can be suppressed by lower temperature operation or through supporting Pt particles on more basic metal oxides. At 50 °C MgO, CeO_2 and $\gamma\text{-}Al_2O_3$, three very different materials in terms of their acidity, surface area, density and crystallinity, appear excellent supports for furfural selective hydrogenation to furfuryl alcohol. There was no evidence of strong metal-support interactions during the liquid phase hydrogenation of furfural, in contrast to that reported for the analogous vapor phase hydrogenation reaction. However, support selection appears critical to achieving the correct platinum dispersion for high furfuryl alcohol yields, with SiO_2 favoring large and broad particle size distributions and concomitant poorer activity and selectivity. All catalysts were found to be recyclable maintaining both activity and selectivity after prolonged testing.

Acknowledgements

GK acknowledges funding from the Royal Society and EPSRC (EP/M005186/1). AFL thanks the EPSRC for a Leadership Fellowship (EP/G007594/4) and KW Royal Society for an Industry Fellowship. MJT acknowledges the award of a PhD scholarship from Hull University.

Appendix A. Supplementary data

Supplementary data associated with this article can be found, in the online version, at http://dx.doi.org/10.1016/j.apcatb.2015.07.006

References

[1] D.A. Bulushev, J.R.H. Ross, Catal. Today 171 (2011) 1–13.
[2] D.A. Simonetti, J.A. Dumesic, ChemSusChem 1 (2008) 725–733.
[3] M.J. Climent, A. Corma, S. Iborra, Green Chem. 16 (2014) 516–547.
[4] C. McGlade, P. Ekins, Nature 517 (2015) 187–190.
[5] M. Chatterjee, H. Kawanami, T. Ishizaka, M. Sato, T. Suzuki, A. Suzuki, Catal. Sci. Technol. 1 (2011) 1466–1471.
[6] A. Mandalika, L. Qin, T.K. Sato, T. Runge, Green Chem. 16 (2014) 2480–2489.
[7] H.S. Luo, H.I. Li, L. Zhuang, Chem. Lett. (2001) 404–405.
[8] M. Pramottana, P. Praserthdam, B. Ngamsom, J. Chin. Inst. Chem. Eng. 33 (2002) 477–481.
[9] K. Egeblad, J. Rass-Hansen, C.C. Marsden, E. Taarning, C. Hviid Christensen, Catalysis, vol. 21, The Royal Society of Chemistry, Cambridge, 2008, pp. 13–50.
[10] A.S. Gowda, S. Parkin, F.T. Ladipo, Appl. Organomet. Chem. 26 (2012) 86–93.
[11] R.V. Sharma, U. Das, R. Sammynaiken, A.K. Dalai, Appl. Catal., A 454 (2013) 127–136.
[12] P.D. Vaidya, V.V. Mahajani, Ind. Eng. Chem. Res. 42 (2003) 3881–3885.
[13] S. Sitthisa, T. Pham, T. Prasomsri, T. Sooknoi, R.G. Mallinson, D.E. Resasco, J. Catal. 280 (2011) 17–27.
[14] S. Sitthisa, W. An, D.E. Resasco, J. Catal. 284 (2011) 90–101.
[15] L.K. Zheng, C.H. Xu, W.B. Liang, J.Y. Liu, J. Liu, X.J. Dun, Y. Guo, Y.C. Yang, Chin. J. Catal. 31 (2010) 461–465.
[16] B.M. Nagaraja, A.H. Padmasri, B. David Raju, K.S. Rama Rao, J. Mol. Catal. A 265 (2007) 90–97.
[17] V.V. Pushkarev, N. Musselwhite, K. An, S. Alayoglu, G.A. Somorjai, Nano Lett. 12 (2012) 5196–5201.
[18] L.R. Baker, G. Kennedy, M. Van Spronsen, A. Hervier, X. Cai, S. Chen, L.-W. Wang, G.A. Somorjai, J. Am. Chem. Soc. 134 (2012) 14208–14216.
[19] K. An, N. Musselwhite, G. Kennedy, V.V. Pushkarev, L.R. Baker, G.A. Somorjai, J. Colloid Interface Sci. 392 (2013) 122–128.
[20] L.J. Durndell, C.M.A. Parlett, N.S. Hondow, M.A. Isaacs, K. Wilson, A.F. Lee, Sci. Rep. 5 (2015).
[21] K. Yan, J. Liao, X. Wu, X. Xie, Adv. Mater. Lett. 4 (2013) 702–707.
[22] A.B. Merlo, V. Vetere, J.F. Ruggera, M.L. Casella, Catal. Commun. 10 (2009) 1665–1669.
[23] A. Merlo, V. Vetere, J. Ramallo-López, F. Requejo, M. Casella, React. Kinet. Mechanism Catal. 104 (2011) 467–482.
[24] P. Mäki-Arvela, L.-P. Tiainen, A.K. Neyestanaki, R. Sjöholm, T.-K. Rantakylä, E. Laine, T. Salmi, D.Y. Murzin, Appl. Catal., A 237 (2002) 181–200.
[25] P.G.N. Mertens, F. Cuypers, P. Vandezande, X. Ye, F. Verpoort, I.F.J. Vankelecom, D.E. De Vos, Appl. Catal., A 325 (2007) 130–139.

[26] L.C. Jones, M.M. Koebel, G.A. Somorjai, J. Nanopart. Res. 10 (2008) 1063–1069.
[27] D. Wang, F. Ammari, R. Touroude, D.S. Su, R. Schlögl, Catal. Today 147 (2009) 224–230.
[28] M. Chen, L.D. Schmidt, J. Catal. 55 (1978) 348–360.
[29] B.K. Min, A.K. Santra, D.W. Goodman, Catal. Today 85 (2003) 113–124.
[30] E.V. Ramos-Fernández, A.F.P. Ferreira, A. Sepúlveda-Escribano, F. Kapteijn, F. Rodríguez-Reinoso, J. Catal. 258 (2008) 52–60.
[31] K. Yan, G. Wu, T. Lafleur, C. Jarvis, Renew. Sust. Energ. Rev. 38 (2014) 663–676.
[32] V. Vetere, A.B. Merlo, J.F. Ruggera, M.L. Casella, J. Braz. Chem. Soc. 21 (2010) 914–920.
[33] N. Merat, C. Godawa, A. Gaset, J. Chem. Technol. Biotechnol. 48 (1990) 145–159.
[34] M. Behrens, G. Lolli, N. Muratova, I. Kasatkin, M. Hävecker, R.N. d'Alnoncourt, O. Storcheva, K. Köhler, M. Muhler, R. Schlogl, Phys. Chem. Chem. Phys. 15 (2013) 1374–1381.
[35] J.M. Bell, D.G. Kubler, P. Sartwell, R.G. Zepp, J. Org. Chem. 30 (1965) 4284–4292.
[36] H. Adkins, E.W. Adams, J. Am. Chem. Soc. 47 (1925) 1368–1381.
[37] N.C. Melchior, J. Am. Chem. Soc. 71 (1949) 3651–3654.
[38] U.K. Singh, M.A. Vannice, J. Catal. 199 (2001) 73–84.